Supplementary Information

Fe_3O_4-functionalized graphene nanosheet embedded phase change material composites: efficient magnetic- and sunlight-driven energy conversion and storage

Wentao Wang, Bingtao Tang,* Benzhi Ju, Zhanming Gao, Jinghai Xiu and Shufen Zhang

State Key Laboratory of Fine Chemicals, Dalian University of Technology, Dalian 116024, China

*E-mail: tangbt@dlut.edu.cn

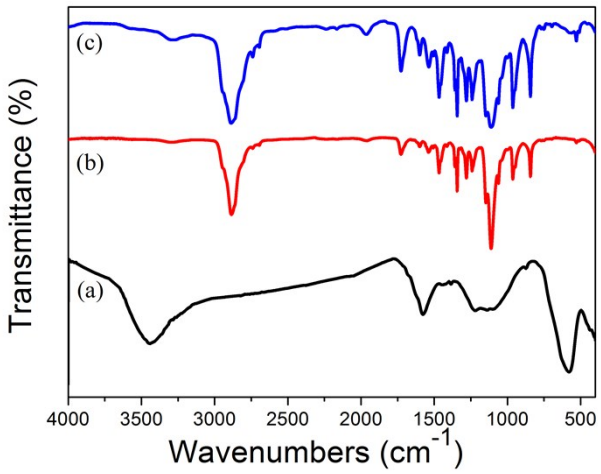

Fig. S1. The FT-IR spectra of (a) Fe_3O_4-GNS synthesized with 10 mmol $FeCl_3$, (b) PCM and (c) Fe_3O_4-GNS/PCM-4.

Fourier transform infrared spectrophotometer was recorded on Thermo Scientific Nicolet 6700 using KBr pellet and Nujol.

Fe_3O_4-GNS (Fig. S8-a): IR (KBr pellet): 1577 (ν C=C), 1219 (ν C-C), 578 (νs Fe-O).

PCM: ITR (Nujol) (Fig. S8-b): 3294 (ν NH), 2885 (ν CH2), 1727(ν C=O), 1599 and 1538(ν C=C aromatic), 1467 (δas CH2), 1359 (νas C-N aromatic), 1343 (δs CH2), 1280 (νas C-O-C), 1241 (νs C-N aromatic), 1112 (νs C-O-C).

Fe_3O_4-GNS/PCM-4: ITR (Nujol) (Fig. S8-c): 3287 (ν NH), 2887 (ν CH2), 1727(ν C=O), 1599 and 1536(ν C=C aromatic), 1467 (δas CH2), 1359 (νas C-N aromatic), 1343 (δs CH2), 1280 (νas C-O-C), 1241 (νs C-N aromatic), 1111 (νs C-O-C).

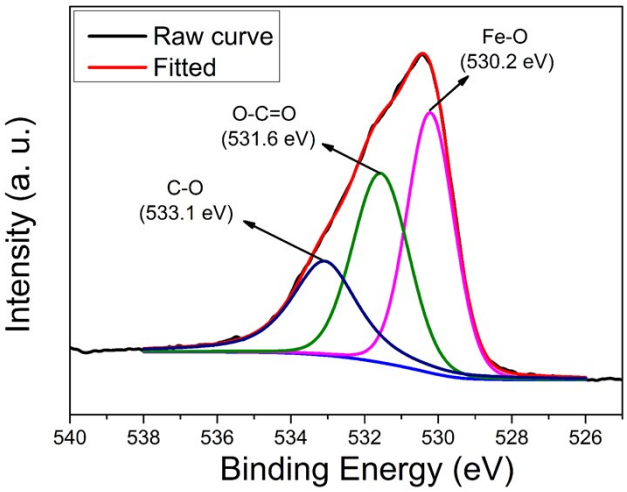

Fig. S2. The O1s spectrum of Fe_3O_4-GNS nanocomposites synthesized with 10 mmol $FeCl_3$.

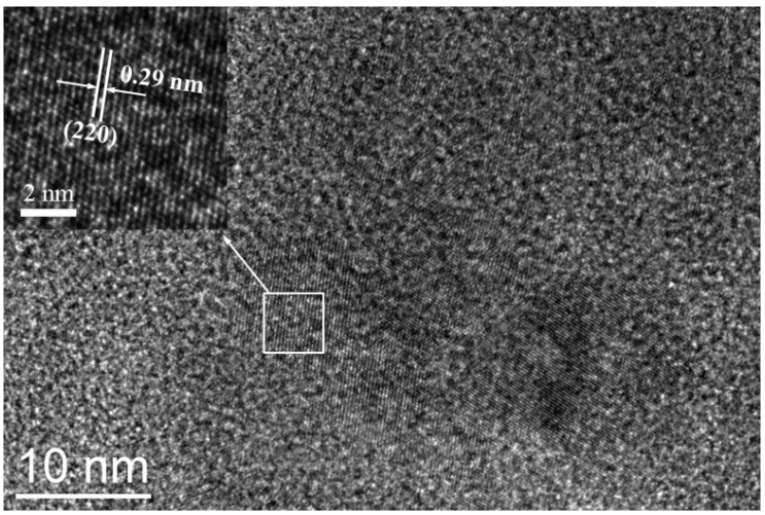

Fig. S3. HRTEM image of Fe_3O_4-GNS nanocomposite synthesized with 10 mmol $FeCl_3$

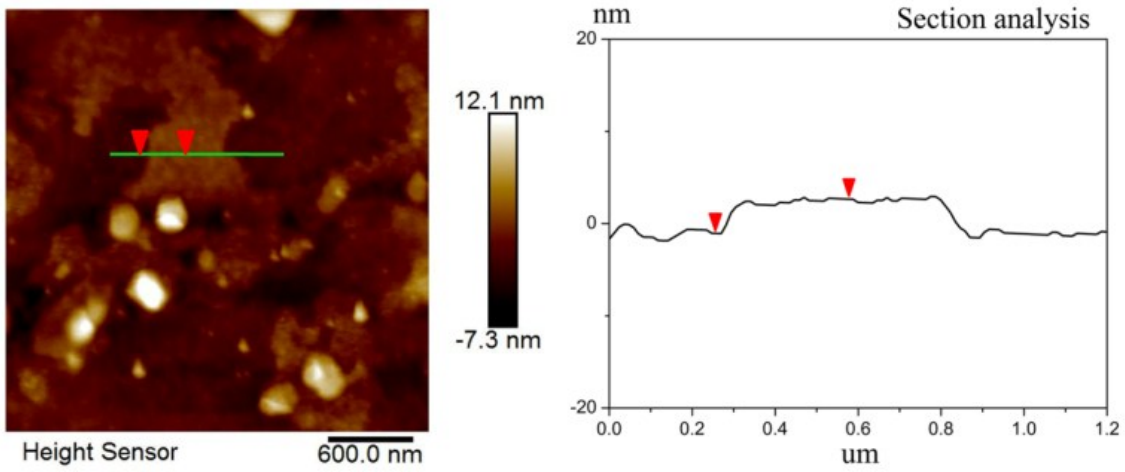

Fig. S4. The AFM image of Fe_3O_4-GNS nanocomposite synthesized with 10 mmol $FeCl_3$.

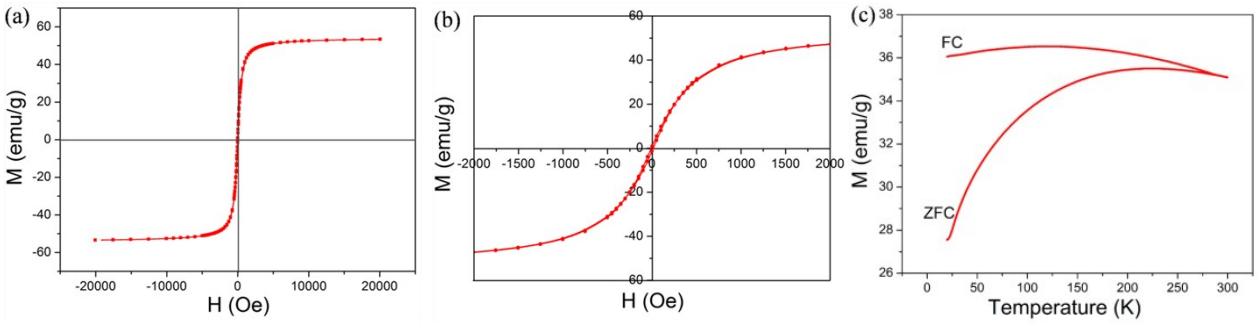

Fig. S5. (a) Room temperature magnetization loops in an applied magnetic field of up to 20 kOe for Fe_3O_4-GNS nanocomposites synthesized with 10 mmol $FeCl_3$, (b) The respective expanded plots for field between 2 k and 2 kOe, (c) The ZFC-FC curves at 500 Oe for Fe_3O_4-GNS nanocomposites synthesized with 10 mmol $FeCl_3$.

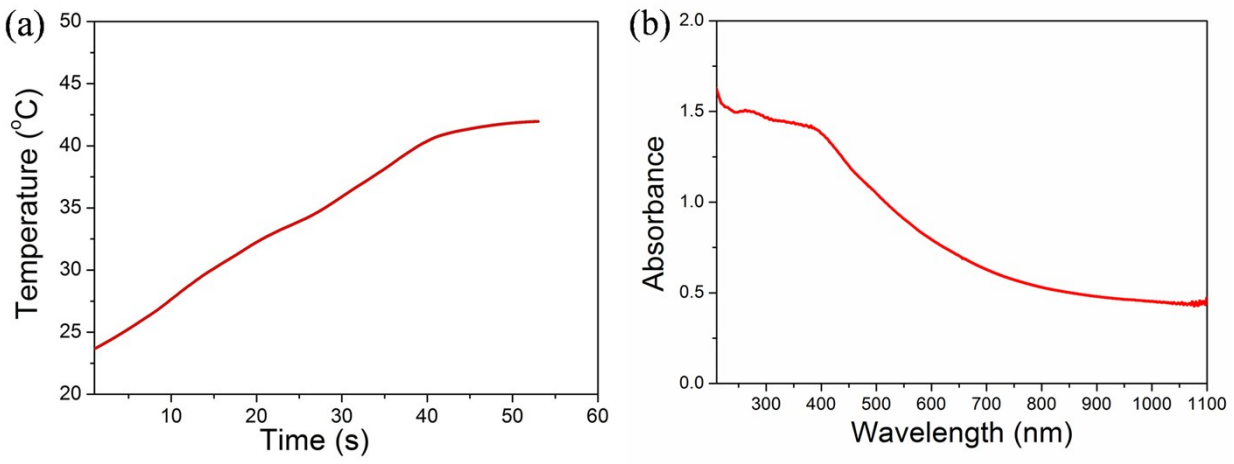

Fig. S6. (a) Magnetothermal measurement under the alternating magnetic field (1.36 MHz, 550 $A \cdot m^{-1}$) for Fe_3O_4-GNS nanocomposites synthesized with 10 mmol $FeCl_3$, (b) UV-vis-NIR absorption spectrum in ethanol (0.06 $mg \cdot mL^{-1}$) for Fe_3O_4-GNS nanocomposites synthesized with 10 mmol $FeCl_3$.

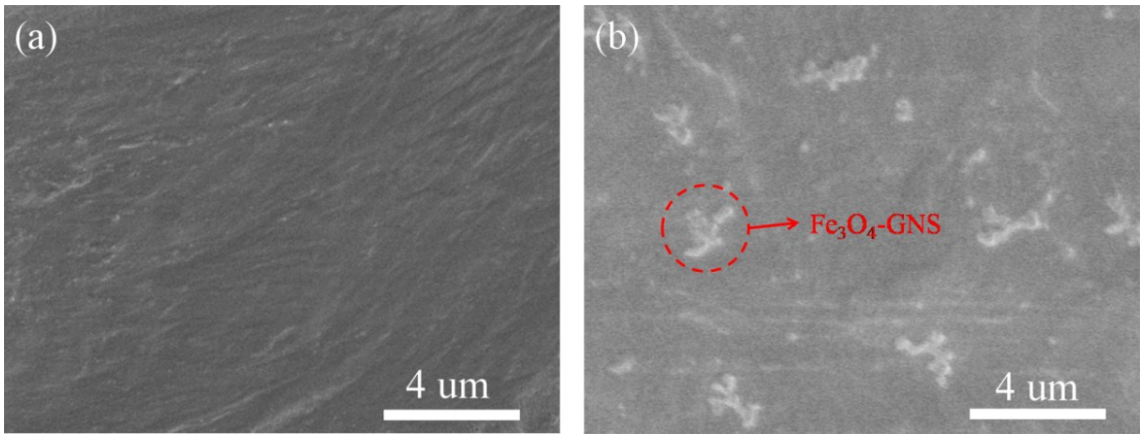

Fig. S7. Cross-sectional SEM images of PCM (a) and Fe_3O_4-GNS/PCM-4 composites (b).

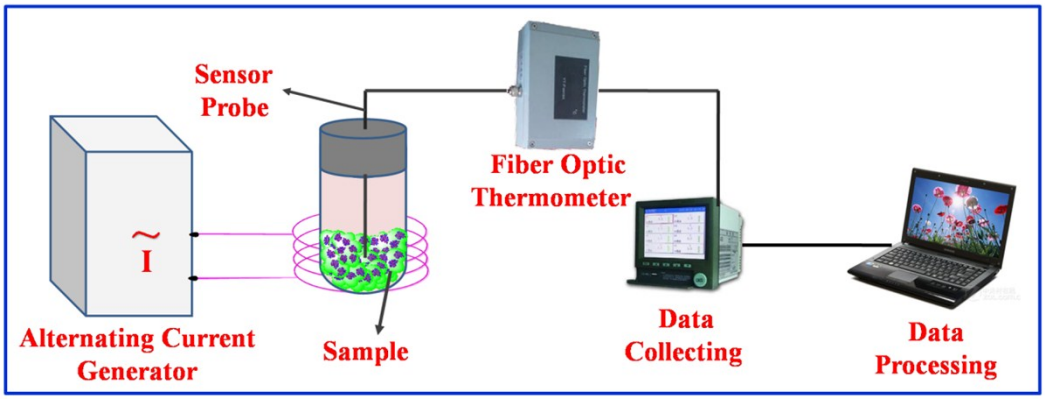

Fig. S8. A schematic of the magnetic-to-thermal energy conversion and storage measuring system.

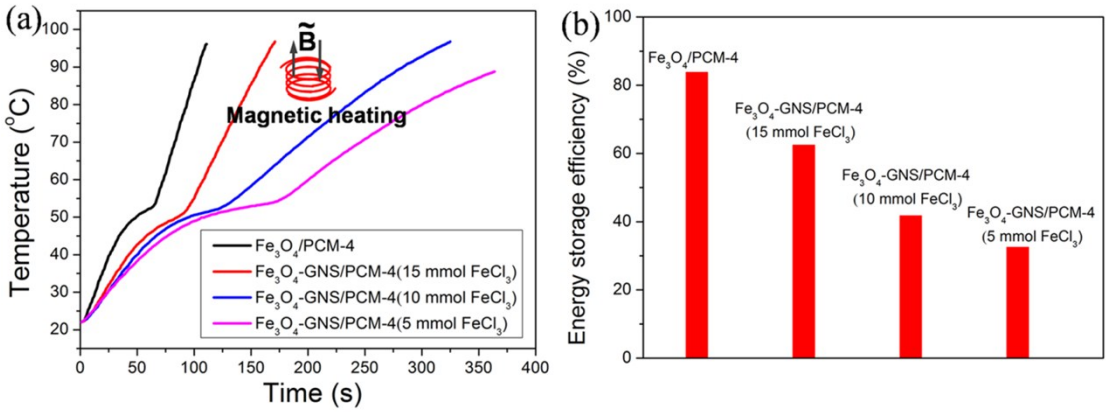

Fig. S9. (a) Magnetic-to-thermal energy conversion curves of the samples (0.5 g) under the alternating magnetic field (1.36 MHz, 550 A·m^{-1}). (b) Calculated magnetic-to-thermal energy storage efficiencies for the Fe_3O_4-GNS/PCM composites with different content of Fe_3O_4 in Fe_3O_4-GNS.

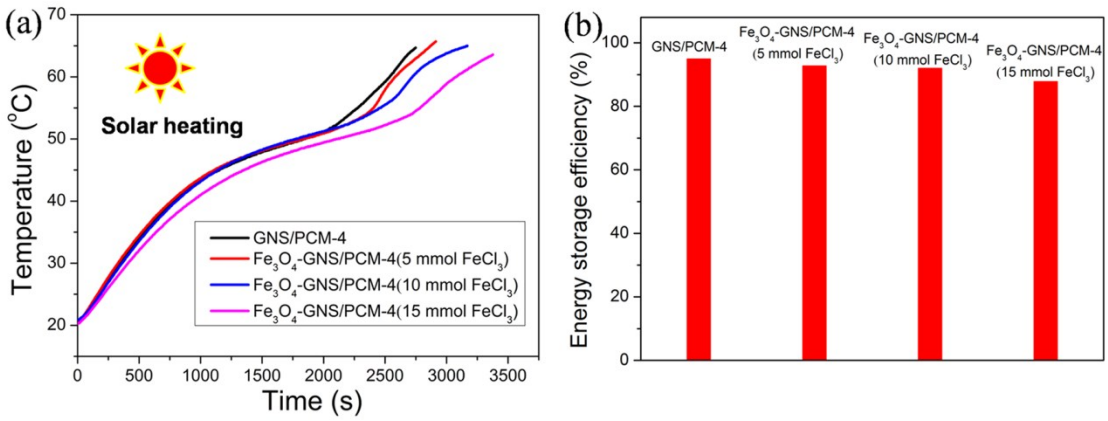

Fig. S10. (a) Solar-to-thermal energy conversion curves of the samples (3.0 g) under sunlight radiation (12:10-13:08, October 5, 2016, P=0.26 W, at an ambient temperature of around 19.5 °C, Dalian, China). (b) Calculated solar-to-thermal energy storage efficiencies for the Fe_3O_4-GNS/PCM composites with different content of Fe_3O_4 in Fe_3O_4-GNS.

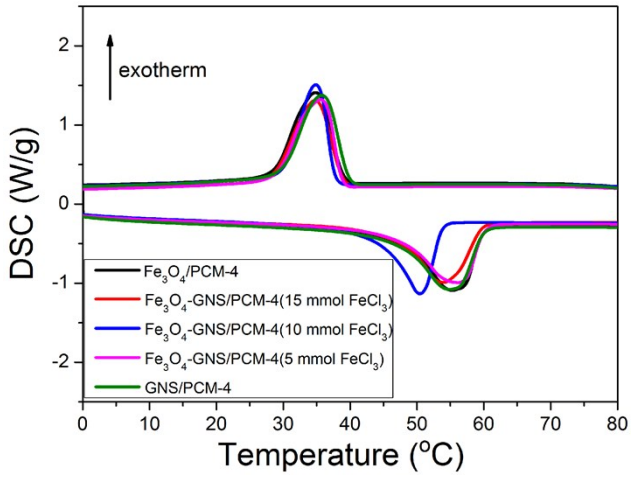

Fig. S11. DSC curves of Fe_3O_4/PCM, GNS/PCM and Fe_3O_4-GNS/PCM with different content of Fe_3O_4 in Fe_3O_4-GNS.

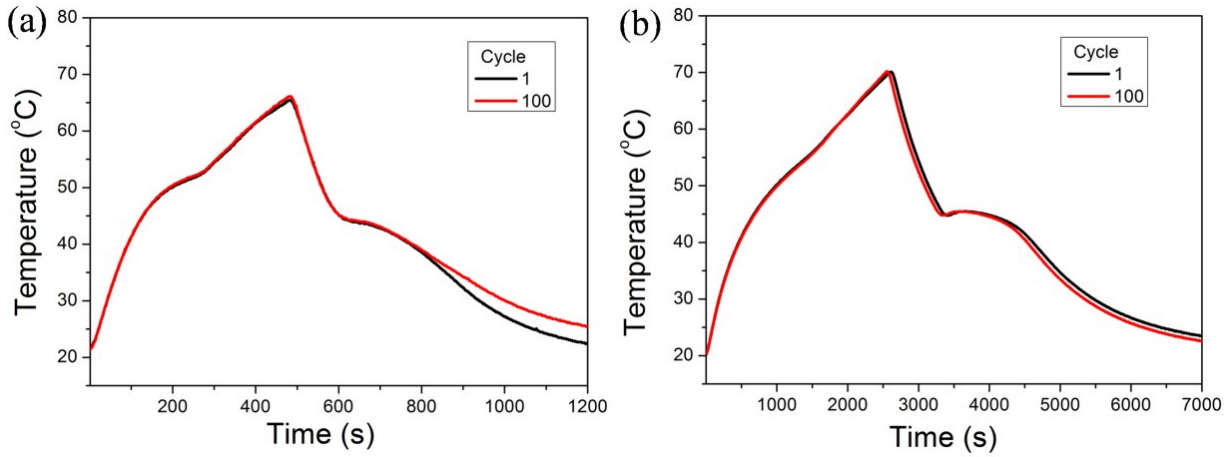

Fig. S12. (a) Magnetic-to-thermal energy conversion curves of Fe_3O_4-GNS/PCM-2 (0.5g) before (black line) and after (red line) 100 cycles of magnetic heating (1.36 MHz, 550 $A \cdot m^{-1}$), (b) Light-to-thermal energy conversion curves of Fe_3O_4-GNS/PCM-2 (3.0 g) before (black line) and after (red line) 100 cycles under simulated sunlight irradiation (P=0.68 W, at an ambient temperature of around 20.5 °C).

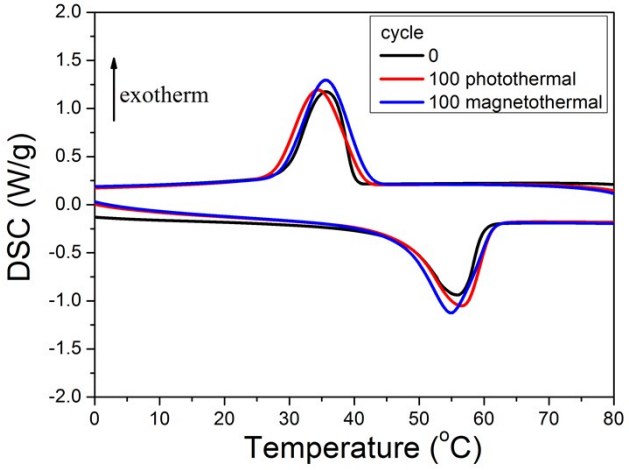

Fig. S13. DSC curves of Fe_3O_4-GNS/PCM-2 before and after 100 magnetothermal and photothermal conversion and storage cycles.

Table S1. Phase change behavior of Fe_3O_4-GNS/PCM-2 before and after 100 magnetothermal and photothermal conversion and storage cycles.

Cycle	ΔH (J/g)		T_r (°C)	
	Heating cycle	Cooling cycle	Heating cycle	Cooling cycle
0	98.8	100.9	55.9	35.5
100 photothermal	101.6	102.1	56.5	34.5
100 magnetothermal	102.6	103.7	55.0	35.6

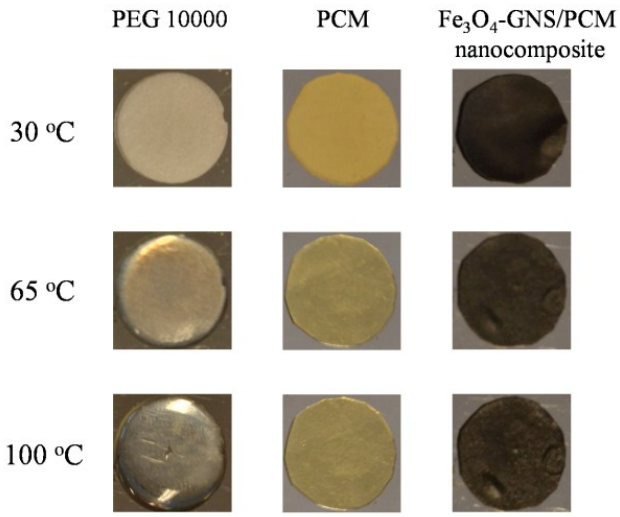

Fig. S14. Macroscopic morphology of the pure PEG, PCM, and Fe_3O_4-GNS/PCM nanocomposites at different temperatures.